# Journal of Materials Chemistry C

Accepted Manuscript


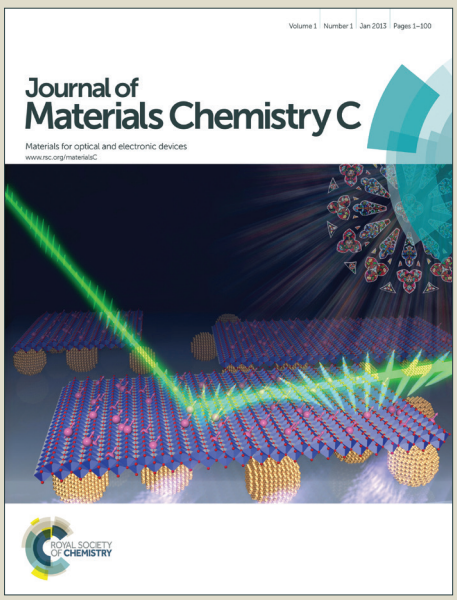





ROYAL SOCIETY OF CHEMISTRY

www.rsc.org/materialsC

Received 00th January 20xx,
Accepted 00th January 20xx

DOI: 10.1039/x0xx00000x

www.rsc.org/

# Atomic Layer Deposition of Transparent Semiconducting Oxide $CuCrO_2$ Thin Films

T. S. Tripathi[a], Janne-Petteri Niemelä[a], Maarit Karppinen[a]*

ABSTRACT: Atomic layer deposition (ALD) is a vital gas-phase technique for atomic-level thickness-controlled deposition of high-quality thin films on various substrate morphologies owing to its self-limiting gas-surface reaction mechanism. Here we report the ALD fabrication of thin films of the semiconducting $CuCrO_2$ oxide that is a highly prospective candidate for transparent electronics applications. In our process, copper 2,2,6,6-tetramethyl-3,5-heptanedionate ($Cu(thd)_2$) and chromium acetyl acetonate ($Cr(acac)_3$) are used as the metal precursors and ozone as the oxygen source. Smooth and homogeneous thin films with an accurately controlled metal composition can be deposited in the temperature range of 240–270 °C; a post-deposition anneal at 700-950°C in an Ar atmosphere then results in well crystalline films with the delafossite structure. Electrical transport measurements confirm the p-type semiconducting behavior of the films. The direct bandgap is determined from UV-vis spectrophotometric measurements to be 3.09 eV. The observed transmittance is greater than 75% in the visible range.

## INTRODUCTION

Copper chromium oxide $CuCrO_2$ is a member of the delafossite family $CuAO_2$ (A = Al, Cr, Fe, Co, Ga, Y, In, La, Nd, and Eu).[1] The basic structural and magnetic properties of $CuCrO_2$ and other members of the family have already been established many years ago. With predominantly antiferromagnetic interactions, members of this family possess a geometrically frustrated triangular lattice. Up until recently the numerous studies published concerning $CuCrO_2$ have been inspired by its large magnetic frustration ($\theta_{CW}/T_N \sim 8$) and the evidence showing that it is multiferroic.[2,3,4,5]

The discovery of simultaneous p-type electrical conductivity and optical transparency in $CuAlO_2$ thin films[6] opened the new venue of research among delafossites for 'invisible electronics'.[7] Subsequently besides the frustrated magnetism, many other $Cu^{+1}$ wide-bandgap triangular-lattice antiferromagnets with the delafossite structure, including $CuInO_2$,[8] $CuScO_2$,[9] $CuGaO_2$,[10] $CuYO_2$ [11] and most recently $CuBO_2$ [12,13] have been investigated as p-type transparent conducting oxides (TCOs). To date the Mg-doped $CuCrO_2$ is reported to have the highest electrical conductivity (220 S $cm^{-1}$) among the delafossite materials.[14]

The need for p-type TCOs stems from the realization of transparent electronics; that by far depends on the p-type semiconductor materials for use in transparent p–n and p–i–n diodes.[15] Materials with a wide bandgap (>3 eV), high electrical conductivity, high mobility, low fabrication cost along with controllable transparency would be a boom for transparent electronics. Thus the research and development of p-type TCOs is a worthwhile endeavor not only to rival the current industry standard n–type TCOs (e.g. $In_{1-x}Sn_xO_3$ and $Al_{1-x}Zn_xO_3$) but also to complement the needs of invisible electronics.

$CuCrO_2$ with a bandgap of >3.0 eV is one of the most prospective p-type candidates for TCO applications, even though the bandgap is yet debatable in the literature with contradictory findings from different groups. Some groups report an indirect bandgap[16,17,18] and others find $CuCrO_2$ to be a direct-bandgap semiconductor.[19] The first measurement of bandgap of $CuCrO_2$ was performed by Benko and Koffyberg[14] who found it to be an indirect bandgap of 1.28 eV with another indirect and direct bandgap allowed transition at 3.08 and 3.35 eV, respectively. Overall the recent optical measurements have found the direct optical bandgap to be in the range of 2.95–3.30 eV estimating $CuCrO_2$ to be transparent to visible light.[20,21,22,23,24,25] It should also be mentioned that besides the TCO applications, $CuCrO_2$ has attracted attention for a range of other applications, ranging from catalysis[26,27,28] and sensors[29,30] to thermoelectrics,[31,32,33] photocatalysis and removal of various hazardous gases[34,35] metal cations.[36]

There are many methods available for the preparation of $CuCrO_2$ thin films and coatings, such as reactive sputtering deposition,[37,38] pulsed laser deposition,[39,40,41,42] chemical solution deposition,[43,44,45,46] and molecular beam epitaxy.[47] However, these techniques may not be vital for the depositions where a precise thickness control (of the order of sub-nanometer) over a large-area and/or nanostructured substrate is required.[48,49]

Atomic layer deposition (ALD)[50] is an advanced thin-film technique that affords precise film-thickness control owing to its unique deposition mechanism based on sequential and repeated

[a]Department of Chemistry, Aalto University, P.O. Box 16100, FI-00076 Aalto, Finland

*maarit.karppinen@aalto.fi

exposure of precursor vapors that undergo self-limiting surface reactions. Not only low deposition temperatures but ALD also offers the benefit of wafer-scale fabrication of various inorganic films, including oxides, nitrides, metals and chalcogenides.[51,52] Here we report the ALD growth of high-quality $CuCrO_2$ thin films; we moreover determine the optical band gap of $CuCrO_2$ in our thin films for the potential application in optoelectronic devices such as flat panel displays and photovoltaics. For these applications the anticipated materials should have optical transmittance greater than 80% of incident light and conductivities greater than $10^3$ S/cm for efficient carrier transport. It is a well-known fact that the transmittance of the films is limited by light scattering at defects and grain boundaries. Hence the employment of ALD may prove useful for these applications with nearly defect-free and homogeneous growth of films.

## EXPERIMENTAL SECTION

Thin films of Cu-Cr-O were deposited from copper 2,2,6,6-tetramethyl-3,5-heptanedionate ($Cu(thd)_2$) and chromium acetyl acetonoate ($Cr(acac)_3$) as metal precursors and ozone as an oxygen source in a commercial hot-wall flow-type F-120 ALD reactor (ASM Microchemistry Ltd., Finland) operated under a nitrogen pressure of 2-3 mbar. Nitrogen (99.9995%) was produced with a NITROX UHPN 3000 nitrogen generator and used both as a carrier and purging gas. $Cr(acac)_3$ (97.5%) was procured from STREM Chemicals whereas $Cu(thd)_2$ was prepared from copper acetate (Fluka; 98%) and 2,2,6,6-tetramethyl hepatane-3,5-dione (Fluka; > 98%) in our laboratory. The sublimation temperature of $Cu(thd)_2$ was determined from thermo-gravimetric (TG) analysis (carried out in air with a heating rate of 10 $^{o}$C/min) and found to be ca. 115 $^{0}$C. The metal precursors $Cu(thd)_2$ and $Cr(acac)_3$ were sublimed from open glass boats held inside the reactor at 120 and 130 °C, respectively. Ozone was produced with a Fischer model 502 laboratory ozone generator from oxygen (99.999%). It was pulsed into the reactor through a needle valve and a solenoid valve from the main ozone flow line. The deposition temperature range studied was from 200 to 270 °C. Pulse and purge lengths for the metal precursors, ozone and N2 purge were initially tested from 1 to 6 s, and then fixed to 2 s for all the three precursors and 3 s for the N2 purge. As commonly observed for ternary oxides the as-deposited films were amorphous;[53,54,55] for crystallization the films were annealed at 500-950$^{0}$C in a rapid thermal annealing (RTA) furnace PEO 601 (ATV Technologie GmbH) in Ar atmosphere.

Most of the films were deposited on 3 × 3 $cm^2$ Si(111) substrates without removing the native oxide layer. However, for the purpose of electrical transport measurements and bandgap determination from UV-vis spectrophotometry data some films were also deposited on borosilicate glass. The dc resistivity was measured in linear four-probe configuration. Seebeck coefficient was measured using our home made setup similar to the setup reported in Ref. 56. The spectrophotometric measurements were performed by Hitachi-U 2000 spectrophotometer in the wavelength range of 190- 1100 nm. Crystal structure of the post-deposition annealed films was identified from grazing incidence X-ray diffraction data (GIXRD; PANanalytical model X'pert Pro diffractometer, Cu Kα radiation). Film thicknesses were determined from X-ray reflectivity (XRR) patterns measured with the same diffractometer. Scanning electron microscopy (SEM; JEOL JSM-7500FA, resolution 0.6 nm @ 30 kV) images were to investigate the surface structures of the films. The surface topography and root mean square (RMS) roughness measurements were performed using an atomic force microscope (AFM, TopoMetrix Explorer). Elemental composition of the films was determined from wavelength dispersive X-ray fluorescence spectroscopy (WD-XRF; PANanalytical Axios$^{mAX}$ microanalysis system equipped with SST-mAX X-ray tube that virtually eliminates instrument drift) and inductively-coupled-plasma optical-emission spectrometry (ICP-OES; Perkin Elmer ICP-OES, 7100 DV) measurements. SuperQ software package from PANanalytical was used for the analysis of the XRF results.

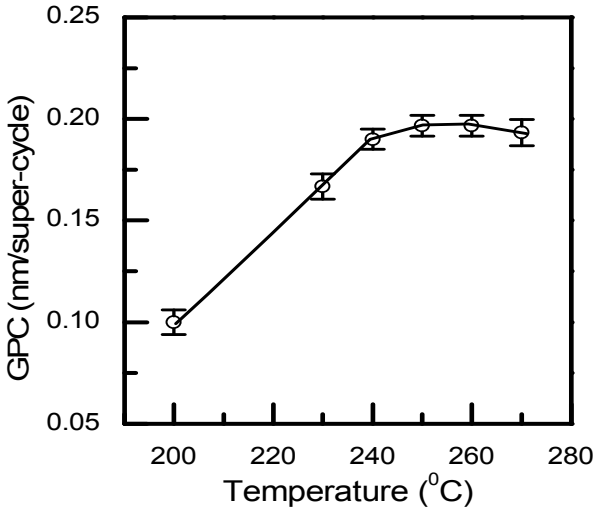


**Figure 1**. Growth per super-cycle (GPC) at different deposition temperatures for films deposited with the sub-cycle ratio of 1:1. The total number of super-cycles is 300.

## RESULTS AND DISCUSSION

First we searched for our new ALD process the temperature range, i.e. so-called ALD window, where the film growth rate remains constant. In Figure 1 the growth per super-cycle (GPC) values for the films at various deposition temperatures from 200 to 270$^{0}$C are plotted. For all these depositions, the ALD super-cycle consisted of the following pulsing sequence: 2 s $Cu(thd)_2$, 2 s ozone, 2 s $Cr(acac)_3$ and 2 s ozone, each precursor pulse followed by an $N_2$ purge of 3 s. The total number of these super-cycles was 300. From Figure 1 the GPC value for our Cu-Cr-O films is essentially constant within 240-270 $^{0}$C; this is a somewhat narrow temperature window considering the ALD windows reported for the binary processes of CuO (190-260 $^{0}$C)[57] and $Cr_2O_3$ (200-280 $^{0}$C)[58] from the same precursors. Beyond 270 $^{o}$C (not shown in the figure) the film growth becomes of the CVD (chemical vapor deposition) type, probably due to decomposition of the precursors. Thus, it was difficult to determine the thickness of the films by XRR measurements. For the further experiments we fixed the deposition temperature to 250 $^{o}$C considering the ALD windows of individual precursors and the temperature range with an essentially constant growth rate from the present depositions.

We confirmed the self-limiting growth behavior with respect to extended precursor pulse (and subsequent purge) lengths by varying these parameters one at a time and keeping all other

deposition parameters fixed. For example to test the self-limiting growth behavior of $Cu(thd)_2$ the pulse (and purge) lengths were varied from 1 s (2 s) to 5 s (6 s) in five separate depositions while the pulse and purge lengths (2 and 3 s) for $Cr(acac)_3$, and $O_3$ remained fixed. The same process was then repeated separately for $Cr(acac)_3$ and $O_3$, see Figure 2. From these experiments it was observed that a pulse (purge) length of 1 s (2 s) was not enough for saturative growth for any of the precursors; a nearly constant growth rate (0.20–0.23 nm/super-cycle) was observed for the pulse (purge) lengths beyond 2 s (3 s). The extended pulse (purge) length beyond 3 s (4 s) for $O_3$ slightly decreased the growth rate probably due to the decomposition of the precursors. Thus we selected the precursor pulse and $N_2$ purge length combination of 2 s and 3 s, respectively, for the rest of the experiments.

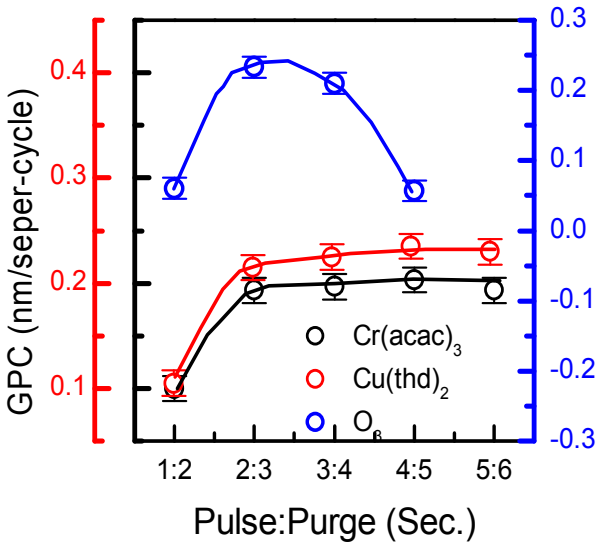


**Figure 2.** Growth per super-cycle (GPC) for various precursor pulse (and subsequent purge) lengths for films deposited with the sub-cycle ratio of 1:1. The total number of super-cycles is 300.

For the initial depositions with the metal precursor cycles in the ratio of 1:1, i.e. $[(Cu(thd)_2 + O_3) + (Cr(acac)_3 + O_3)]$, the cation molar ratio Cu/Cr determined from the XRF and ICP measurement data was always larger than 1.5. Thus to get the desired molar ratio, i.e. Cu/Cr = 1.0, the number of $(Cr(acac)_3 + O_3)$ sub-cycles in the super-cycle was increased from 1:1 to 1:2 and 1:3. In the 1:2 case the resultant Cu/Cr molar ratio was determined to be ca. 1.3, while in the 1:3 case a Cu/Cr ratio (i.e. 1.02) equal to the target stoichiometry within experimental error was achieved. Hence we fixed the ALD super-cycle for our remaining experiments to be: $[(Cu(thd)_2 + O_3) + 3 \times (Cr(acac)_3 + O_3)]$. At the deposition temperature of 250 $^{o}$C the GPC for this super-cycle was found to be 0.55 nm / super-cycle. In Figure 3 we plot the film thickness against the number of super-cycles deposited at 250 $^{o}$C with the sub-cycle ratio of 1:3; it is seen that the film growth is essentially linear as expected for a well-behaving ALD process.

In Figure 4 we show XRD patterns and SEM images for the films with the stoichiometric Cu/Cr ratio after annealing the as-deposited films at different temperatures in an Ar atmosphere for 10 minutes. The as-deposited film is non-crystalline and as expected the crystallinity of the films enhances with increasing annealing temperature. The film annealed at 700 $^{0}$C contains small proportions of CuO and $CuCr_2O_4$ phases along with the $CuCrO_2$ phase. By 800 $^{0}$C the CuO and $CuCr_2O_4$ phases have transformed to $CuCrO_2$, however, annealing the films further at 950 $^{0}$C improves the crystallinity and a phase-pure $CuCrO_2$ film is obtained. The SEM images reveal that the as-deposited non-crystalline film has a smooth homogeneous surface. For the film annealed at 500 $^{0}$C appearance of polygon-like irregular grains is seen with the typical grain size in the range of 20-80 nm. Grains for the film annealed at 700$^{0}$C are somewhat larger but diffused and have irregular shapes probably due to the mixed-phase nature of the film, while the grains in the film annealed at 950$^{0}$C are smaller but distinct and have almost regular rod-like shapes of approximately 130 nm long. The mixture of bar- and polygonal-like features in the film annealed at 950 $^{o}$C is attributed to the delafossite structure successfully forming during the annealing process. Hence we may conclude that our XRD and SEM data are in excellent agreement.

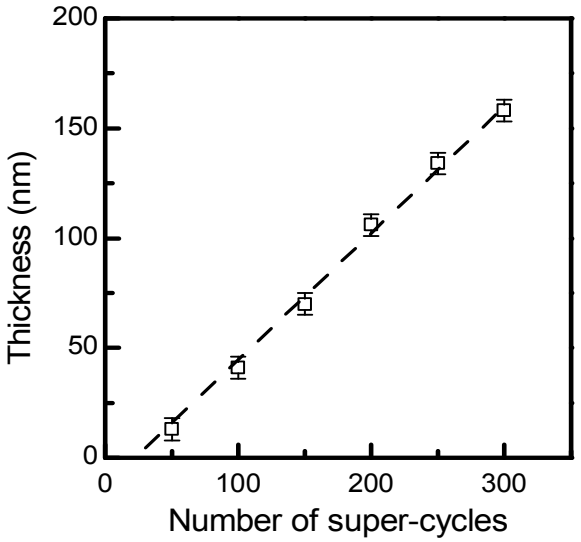


**Figure 3.** Film thickness versus number of super-cycles for films deposited with the sub-cycle ratio of 1:3, i.e. $[(Cu(thd)_2 + O_3) + 3 \times (Cr(acac)_3 + O_3)]$. The deposition temperature is 250 $^{o}$C.

In Figure 5 we show the surface topography and root mean square (RMS) roughness features of the films measured by AFM. In line with the XRD and SEM data the surface topography and roughness of the films change due structural and phase changes driven by different annealing temperatures. The as-deposited non-crystalline film (Figure 5a) shows the minimum RMS roughness value of 0.98 nm. As shown in Figure 5(b, c and d), the RMS roughness of the films increases from 1.46 to 2.65 nm with increasing annealing temperature. This shows the improved crystallinity of the films with temperature. The RMS roughness values of the 700 $^{0}$C-annealed film is a little more than the single-phase 950 $^{0}$C annealed film. We believe that this may be related to the mixed compositions of CuO and $CuCr_2O_4$ phases as observed in XRD and SEM measurements. Similar roughness features have been observed in magnetron sputtered Cu-Cr-O films at different annealing temperatures.[61]

In Figure 6 we show the electrical transport measurements on the films (thickness 150 nm) annealed at various temperatures

600-800 $^{0}$C. The T dependence of resistivity shows a purely semiconducting behavior with $d\rho/dT < 0$ as the temperature is increased. With higher annealing temperature, resistivity of the films decrease probably due to increased carrier density and conversion of remnant CuO and $CuCr_2O_4$ to $CuCrO_2$.[61] The resistivity of the films matches well with the values reported in literature.[15,61] The inset of figure 6 shows the room temperature Seebeck coefficient of the same films. The positive Seebeck coefficient confirms the p-type conductivity of the films. Quantitatively Seebeck values do not change much with higher annealing temperature however show a linear increasing trend with values ~ 300±10 μV/K at room temperature. This is comparable (~ 350 μV/K) to the value reported by T. Okuda et al.[31-33] for powder samples of Mg doped $CuCrO_2$. However, much higher (~ 1200 μV/K) values have been reported by Benko, Koffyberg[16] and Y. Ono et al.[32] for bulk powdered samples of Ca and Mg doped $CuCrO_2$ respectively. This is believed to be related to the large resistivity differences[14] of their materials (~ 100 Ω cm) to the films we measured (~ 1.0 Ω cm).

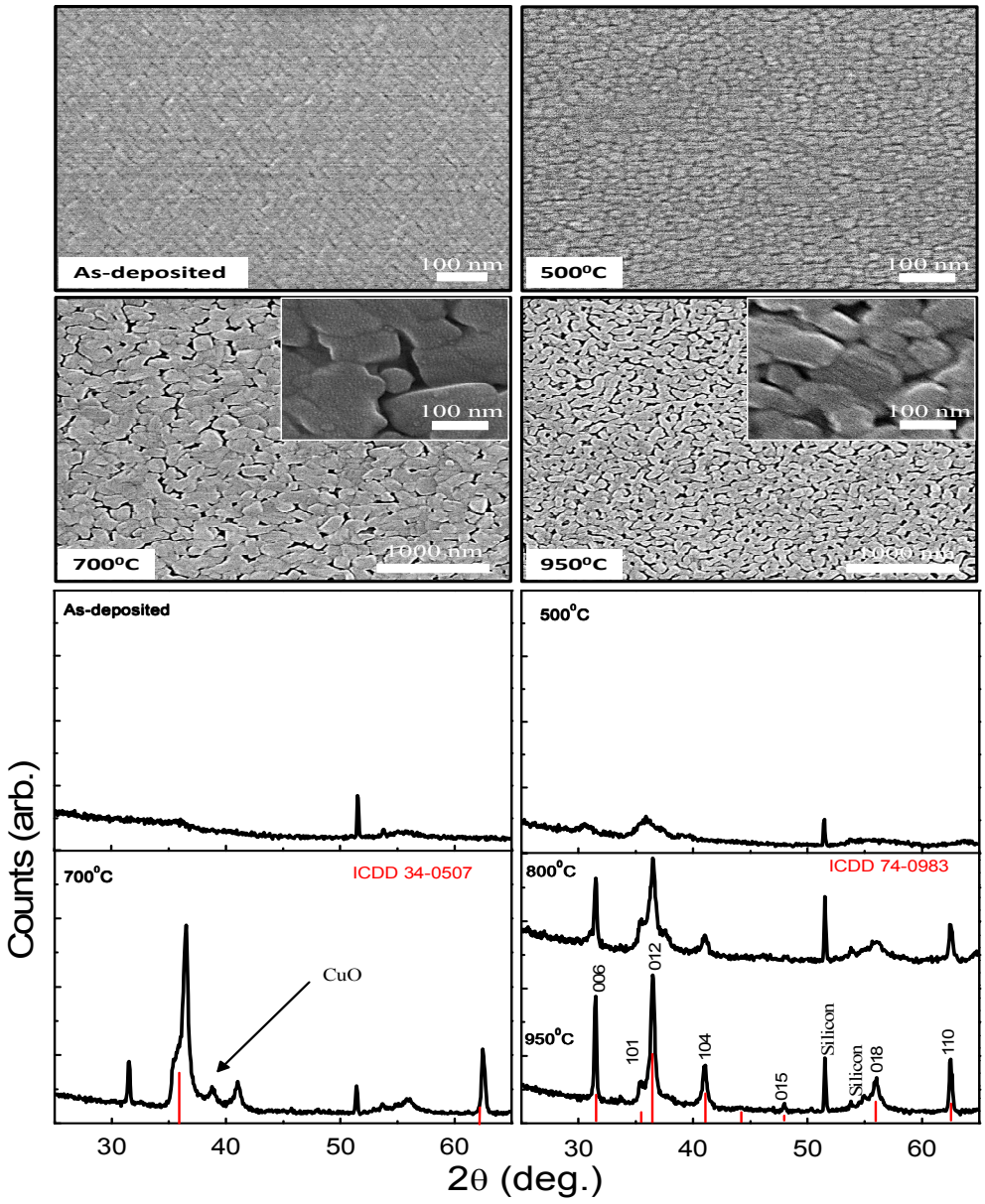


**Figure 4.** XRD patterns and SEM images for an as-deposited $CuCrO_2$ film and films annealed in Ar at 500, 700, 800 and 950 $^{0}$C. Red lines show the diffraction peaks matched with ICDD reference data for $CuCrO_2$ (ICDD 74-0983) and $CuCr_2O_4$ (ICDD 37-0507).

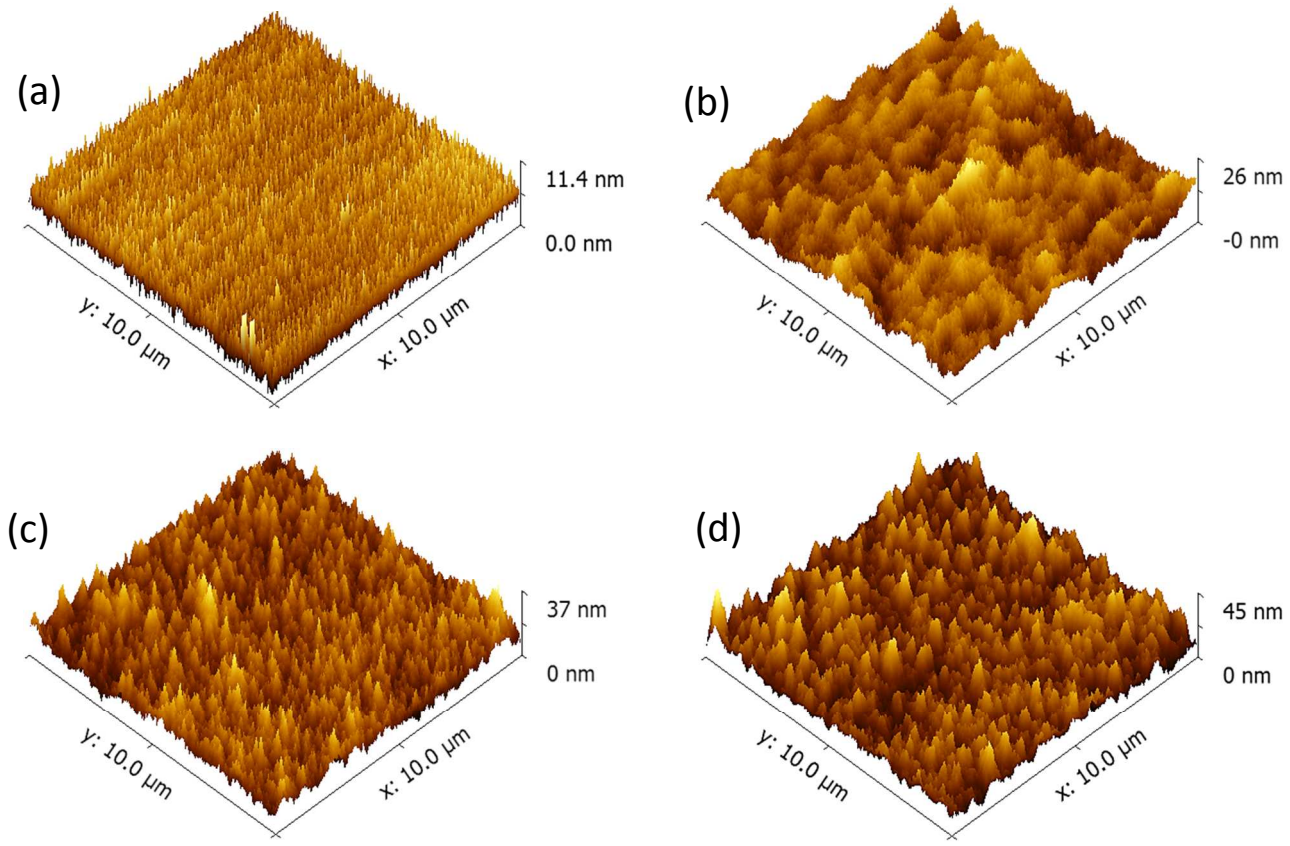


**Figure 5.** Atomic force microscopy images of **(a)** as-deposited film (RMS = 0.98 nm), **(b)** 500 $^0$C (RMS = 1.46 nm), **(c)** 700 $^0$C (RMS = 2.65 nm) and **(d)** 950 $^0$C (RMS = 2.46 nm) annealed films in Ar atmosphere for 10 min.

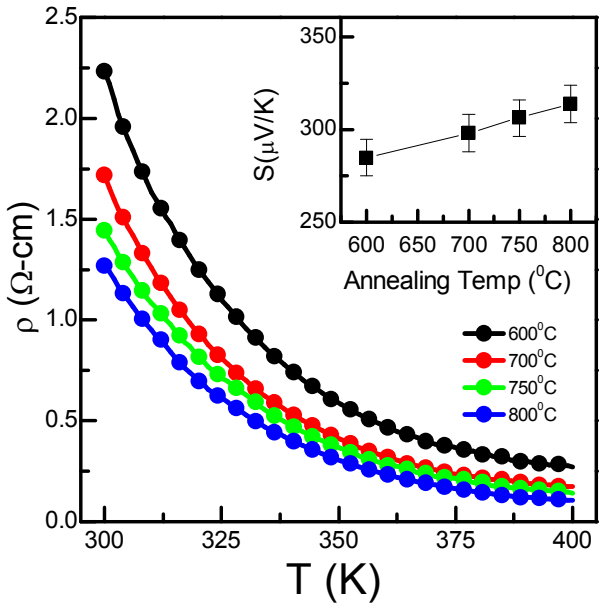


**Figure 6.** Temperature dependence of resistivity of the films for various annealing temperatures. The inset shows the Seebeck values of the same films at room temperature.

Finally, in Figure 7 we display the UV-vis spectra measured for an 800 $^o$C annealed $CuCrO_2$ film deposited on a borosilicate glass substrate. Thickness of the film is 150 nm. Figure 7(a) shows the wavelength dependence of transmittance and reflectance data for the film and for the plain borosilicate glass substrate. The film has a light transmittance of approximately 72–79 % at wavelengths of 600–800 nm, respectively, being slightly better than the values (60-75 %) reported in literature for $CuCrO_2$ films deposited by a sol-gel technique.[59,60] From the film's light transmittance and reflectance data the absorption coefficient $\alpha$ can be calculated at each wavelength as follows:

$$\alpha = \left(\frac{1}{d}\right) ln\left(\frac{1-R}{T}\right) \quad (1)$$

where d is the thickness, R is the reflectance and T is the light transmittance of the film.

The inset of Figure 7(b) shows the absorption coefficient as a function of wavelength. The absorption curve rises sharply (characteristic absorption) and shows a peak (marked as I) located at wavelength 350 nm corresponding to incident photon energy of 3.54 eV.

Journal Name

ARTICLE

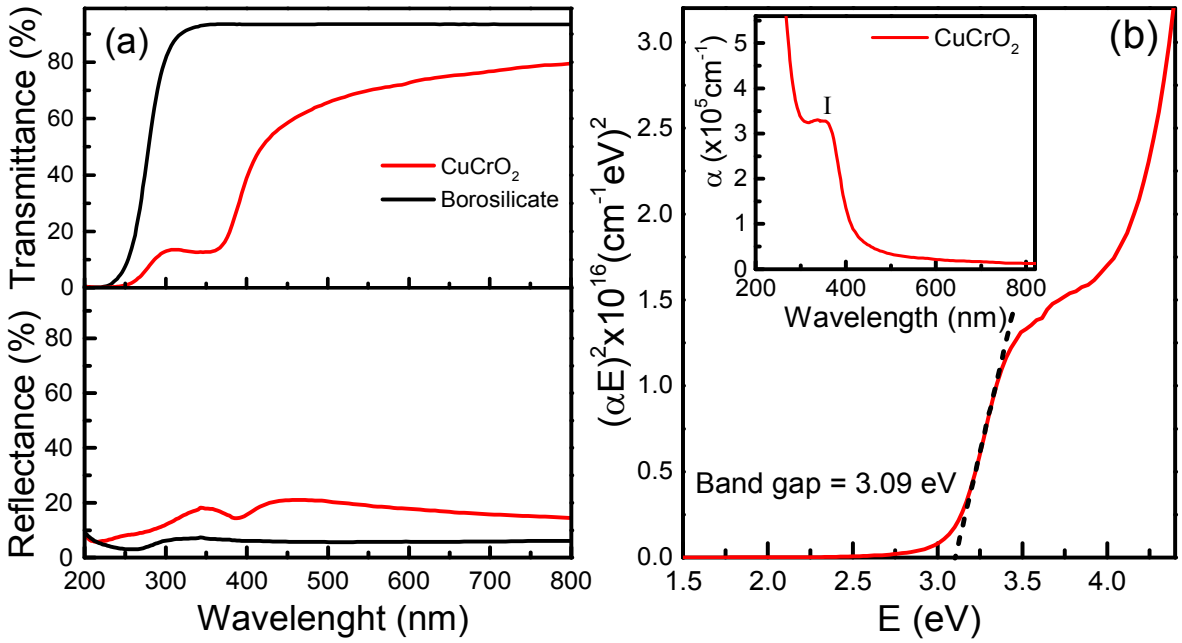


**Figure 7.** (a) Transmittance and reflectance spectra for an annealed crystalline $CuCrO_2$ film deposited on a borosilicate glass substrate. (b) Direct bandgap of the film. Inset shows the absorption coefficient as a function of wavelength.

Such peaks have been mentioned to appear as sub-bandgap transitions[61] when the relationship, $h\nu = E_g - E_k$ between an incident photon and a free exciton in the semiconductor is satisfied.[62]

Here $h\nu$ is the incident photon energy, $E_g$ is the bandgap and $E_k$ is the binding energy of the free exciton and k represents the wave-vector on the E–k diagram. On E–k diagram, sub-bands lie at lower energy positions. Thus sub-bandgap transitions are not, in general, capable of creating hole carriers to make any appreciable contribution to the electrical conductivity.

The following equation is used frequently to estimate the bandgap of a semiconductor material:

$$(\alpha h\nu)^{1/n} = A(h\nu - E_g) \quad (2)$$

where $\alpha$ is the absorption coefficient and A is an arbitrary constant. For direct and indirect bandgaps n is taken as ½ and 2, respectively. From the graph $(\alpha h\nu)^2$ versus $h\nu$ the direct bandgap of a material can be determined. As shown in Figure 7(b) the direct bandgap of our ALD $CuCrO_2$ film is estimated to be 3.09 eV. The obtained values are consistent with direct bandgaps of 2.95–3.55 eV reported in previous studies.[20-25]

## CONCLUSIONS

In this work, we developed an atomic layer deposition process to fabricate $CuCrO_2$ thin films. Though the study was particularly intended to the growth of high-quality $CuCrO_2$ films the information of the process parameters and growth characteristics may also be useful for the deposition of other members of the $CuAO_2$ delafossite family for potential TCO applications. Our ALD process is based on $Cu(thd)_2$, $Cr(acac)_3$ and ozone precursors, and to get the desired Cu/Cr ratio for $CuCrO_2$ a super-cycle was employed with one $Cu(thd)_2$-$O_3$ and three $Cr(acac)_3$-$O_3$ sub-cycles. The ALD temperature window was found at 240-260 $^{o}$C. The as-deposited films exhibited smooth homogeneous surfaces but were non-crystalline; annealing at 800-950 $^{0}$C in Ar then revealed crystalline $CuCrO_2$ films for which highly promising optical characteristics could be measured, i.e. transmittance values greater than 75% in the visible range with the direct bandgap of 3.09 eV. One higher-energy sub-band transition was observed at 3.54 eV. Electrical transport measurements confirm the p-type semiconducting behavior of the films.

## ACKNOWLEDGMENTS

The present work has received funding from the European Research Council under the European Union's Seventh Framework Programme (FP/2007-2013)/ERC Advanced Grant Agreement (No. 339478) and also from the Aalto Energy Efficiency Research Programme.

REFERENCES


1 D. B. Rogers, R. D. Shannon, C. T. Prewitt, and J. L. Gillson, *Inorg. Chem*. 1971, **10**, 723.

2 S. Seki, Y. Onose and Y. Tokura, *Phys. Rev. Lett*., 2008, **101**, 067204.

3 K. Kimura, H. Nakamura, S. Kimura, M. Hagiwara, and T. Kimura, *Phys. Rev. Lett*., 2009, **103**, 107201.

4 O. S. Yamaguchi, H. S. Kimura, M. Hagiwara, K. Kimura, T. Kimura, T. Okuda and K. Kindo, *Phys. Rev. B,* 2010, **81**, 033104.

5 M. Poienar, F. Damay, C. Martin, V. Hardy, A. Maignan and G. Andre, *Phys. Rev. B,* 2009, **79**, 014412.

6 H. Kawazoe, M. Yasukawa, H. Hyodo, M. Kurita, H. Yanagi, and H. Hosono, *Nature* (London), 1997, **398**, 939.

5 G. Thomas, *Nature* (London), 1997, **389**, 907.

8 H. Yanagi, T. Hase, S. Ibuki, K. Ueda, H. Hosono, *Appl. Phys. Lett,.* 2001, **78**, 1583.

9 N. Duan, A. W. Sleight, M. K. Jayaraj, and J. Tate, *Appl. Phys. Lett.,* 2000 **77**, 1325.

10 H. Kawazoe, H. Yanagi, K. Ueda, and H. Hosono, *MRS Bull*., 2000, **25**, 28.

11 R. Nagarajan, N. Duan, M. K. Jayaraj, J. Li, K. A. Vanaja, A. Yokochi, A. Draeseke, J. Tate, and A. W. Sleight, *Int. J. Inorg. Mater.*, 2001, **3**, 265–270.

12 M. Snure and A. Tiwari, *Appl. Phys. Lett.*, 2007, **91**, 092123.

13 D. O. Scanlon, A. Walsh, and G. W. Watson, *Chem. Mater.*, 2009, **21**, 4568–4576.

14 R. Nagarajan, A. D. Draeseke, A. W. Sleight, and J. Tate, *J. Appl. Phys.*, 2001, **89**, 8022.

15 J. Tate, M. K. Jayaraj, A.D. Draeseke, T. Ulbrich, A.W. Sleight, K. A. Vanaja, R. Nagarajan, J. F. Wager, and R. L. Hoffman, *Thin Solid Films*, 2002, **411,** 119.

16 F. A. Benko and F. P. Koffyberg, *Mater. Res. Bull*., 1986, **21**, 753–757.

17 A. C. Rastogi, S. H. Lim, and S. B. Desu, *J. Appl. Phys.*, 2008, **104**, 032712.

18 S. Mahapatra and S. A. Shivashankar, *Chem. Vap. Deposition*, 2003, **9**, 238–240.

19 D. Li, X. D. Fang, Z. H. Deng, S. Zhou, R. H. Tao, W. W. Dong, T. Wang, Y. P. Zhao, G. Meng, and X. B. Zhu, *J. Phys. D: Appl. Phys*., 2007, **40**, 4910–4915.

20 D. O. Scanlon and G. W. Watson, *J. Mater. Chem*., 2011, **21**, 3655.

21 P.W. Sadik, M. Ivill, V. Craciun, and D. P. Norton, *Thin Solid Films*, 2009, **517**, 3211–3215.

22 R. Bywalez, S. Gotzendorfer, and P. Lobmann, *J. Mater. Chem.,* 2010, **20**, 6562–6570.

23 W. T. Lim, L. Stafford, P. W. Sadik, D. P. Norton, S. J. Pearton, Y. L. Wang, and F. Ren, *Appl. Phys. Lett.*, 2007, **90**, 142101.

24 S. Zhou, X. Fang, Z. Deng, D. Li, W. Dong, R. Tao, T. Meng, and X. Zhu, *J. Cryst. Growth*, 2008, **310**, 5375–5379.

25 M. O'Sullivan, P. Stamenov, J. Alaria, M. Venkatesan, and J. M. D. Coey, *J. Phys.: Conf. Ser.*, 2010, **200**, 052021.

26 Y. Ma, X. Zhou , Q. Ma, A. Litke, P. Liu, Y. Zhang, C. Li, and E. J. M. Hensen, *Catal Lett*, 2014, **144**, 1487–1493.

27 A. P. Amrute, G. O. Larraz_bal, C. Mondelli, and J. P_rez-Ram, *Angew. Chem. Int. Ed*., 2013, **52**, 9772 –9775.

28 R. Rao, A. Dandekar, R. T. K. Baker, and M. A. Vannice, *J. Catal*., 1997, **171**, 406–429.

29 S. Zhou, X. Fang, Z. Deng, D. Li, W. Dong, and R. Tao, *Sensors and Actuators B*, 2009, **143**, 119.

30 Z. Deng, X. Fang, D. Li, S. Zhou, R. Tao, W. Dong, T. Wang, G. Meng, and X. Zhu, *J. Alloys Compd.*, 2009, **484**, 619–621.

31 T. Okuda, N. Jufuku, S. Hidaka, and N. Terada, *Phys. Rev. B*, 2005, **72**, 144403.

32 Y. Ono, K. Satoh, T. Nozaki, and T. Kajitani, *Jpn. J. Appl. Phys.*, 2007 **46**, 1071–1075.

33 K. Hayashi, K. Sato, T. Nozaki, and T. Kajitani, *Jpn. J. Appl. Phys*., 2008, **47**, 59–63.

34 S. Saadi, A. Bouguelia, and M. Trari, *Sol. Energy*, 2006, **80**, 272–280.

35 W. Ketir, A. Bougu, and M. Trari, *Desalination*, 2009, **244**, 144–152.

36 W. Ketir, A. Bouguelia, and M. Trari, *J. Hazard. Mater.*, 2008, **158**, 257–263.

37 G. B. Dong, M. Zhang, X. P. Zhao, H. Yan, C. Y. Tian, and Y. G. Ren, *Appl. Surf. Sci*., 2010, **256**, 4121-4124.

38 H. Sun, M. A. P. Yazdi, P. Briois, J. F. Pierson, F. Sanchette, and A. Billard, *Vacuum*, 2015, **114,** 101-107.

39 X. S. Zhou, F. T. Lin, W. Z. Shi, A. Y. Liu, *J. Alloys Compd*., 2014, **614**, 221-225.

40 D. Li, X. D. Fang, Z. H. Deng, S. Zhou, R. H. Tao, W. W. Dong, T. Wang, Y. P. Zhao, G. Meng, and X. B. Zhu, *J. Phys. D: Appl. Phys.*, 2007, **40,** 4910–4915.

41 P. W. Sadik, M. Ivill, V. Craciun, and D. P. Norton, *Thin Solid Films*, 2009, **517**, 3211.

42 S. Y. Kim, S. Y. Sung, K. M. Jo, J. H. Lee, J. J. Kim, S. J. Pearton, D. P. Norton, Y. W. Heo, *J. Crystal Growth*, 2011, **326** 9.

43 Y. F. Wang, Y. J. Gu, T. Wang, W. Z. Shi, *J Sol-Gel Sci Technol*, 2011, **59**, 222-227.

44 S. Mahapatra, S. A. Shivashankar, *Chem. Vap. Deposit*., 2003, **9**, 238.

45 H. Y. Chen, K. P. Chang, C. C. Yang, *Appl Surf Sci.*, 2013 **273**, 324-329.

46 H. Y. Chen, K. P. Chang, C. C. Yang, *Appl. Surf. Sci.*, 2013, **273**, 324-329.

47 D. Shin, J. S. Foord, R. G. Egdell, and A. Walsh, *J. Appl. Phys*., 2012, **112**, 113718.

48 S.-Å. Lindgren and L. Walldén '*Some properties of metal overlayers on metal substrates*' Chapter 13 handbook of surface science volume 2, Electronic Structure by K. Horn and M. Scheffer. Published by Newnes, (2000).

49 D. A. Luh, T. Miller, J. J. Paggel, and T. C. Chiang, *Phys. Rev. Lett.*, 2002, **88**, 256802.

50 S. M. George, *Chem. Rev.*, 2010, **110**, 111.

G. N. Parsons, J. W. Elam, S. M. George, S. Haukka, H. Jeon, W. M. M. Kessels, M. Leskelä, P. Poodt, M. Ritala and S. M. Rossnagel, *J. Vac. Sci. Technol. A*, 2013, **31**, 050818.

51 J. E. Crowell, *J. Vac. Sci. Technol. A,* 2003, **21**, S88; V. Miikkulainen, M. Leskelä, M. Ritala, and R. L. Puurunen, *J. Appl. Phys.*, 2013, **113**, 021301.

52 J. S. Ponraj, G. Attolini, and M. Bosi, *Crit. Rev. Solid State Mater. Sci.*, 2013, **38**, 203.

53 K. Uusi-Esko, J. Malm, and M. Karppinen, *Chem. Mater.*, 2009, **21**, 5691 - 5694.

54 K. Uusi-Esko, E.-L. Rautama, M. Laitinen, T. Sajavaara, and M. Karppinen, *Chem. Mater.*, 2010, **22,** 6297 - 6300.

55 K. Uusi-Esko, M. Karppinen*, Chem. Meter.*, 2011, **23**, 1835- 1840.

56 T. S. Tripathi, M. Bala,and K. Asokan, *Rev. Sci. Instrum.*, 2014, **85**(8), 085115

57 P. Mårtensson and J.-O. Carlsson, *J. Electrochem. Soc.*, 1998, **145**, 2926–2931.

58 S. Haukka, E.-L. Lakomaa, and T. Suntola, *Appl. Surf. Sci.*, 1994, **75**, 220.

59 H. Y. Chen and K. P. Chang, *ECS J. Solid State Sci. Technol.*, 2013, **2**, P76.

60 S. Götzendörfer, C. Polenzky, S. Ulrich, and P. Löbmann, *Thin Solid Films*, 2009, **518**, 1153.

61 R. S. Yu and C. M. Wu, *Appl. Surf. Sci.*, 2013, **282**, 92–97.

62 J. I. Pankove, Optical Processes in Semiconductors, Prentice-Hall Inc., Englewood Cliffs, NJ, 1971, pp. 57.

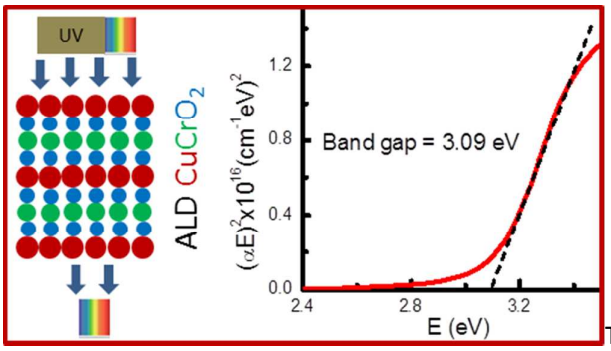


TOC Figure